PLANAR GRID OSCILLATORS FOR QUASI-OPTICAL POWER COMBINING AT 37 GHz

A. Torabi, H. M. Harris, R. W. McMillan, S. M. Halpern, J. C. Wiltse, D. Gagnon[1], D. W. Griffin[2] and C. J. Summers
Electro-Optics and Physical Sciences Laboratory
Georgia Tech Research Institute
Atlanta, Georgia 30332

Abstract

We have investigated a planar grid array of HEMTs placed in a semi-confocal open resonator to explore quasi-optical power combining at Ka-band. The grids were designed for 38 GHz, 30 GHz, and 25 GHz and they operated at 37.4 GHz, 29.3 GHz and 24.8 GHz, respectively. Under the conditions of these tests, the grid geometry is the dominant factor in setting the frequency of oscillation. We have measured 8 mW from a column of three devices placed in a grid with at least 6% DC to RF conversion efficiency.

Introduction:

Solid state semiconductor millimeter wave (MMW) sources are small, inexpensive, lightweight, operate at low power, can operate up to terahertz frequencies, and can be integrated into circuits with a large number of devices. To achieve high output power, it is necessary to combine the power from these sources. Ideally such combiners should accommodate a large number of devices in the form of a compact array that operates as a synchronized assembly free of multimoding problems.

An attractive scheme for power combining has been suggested by Mink (1) and has been studied by several investigators (2-4) at frequencies up to Ku-band. In this technique, single devices are embedded in a two dimensional array such that they operate and produce a uniformly coherent beam perpendicular to the array. The array is placed in a Fabry-Perot resonator to provide the feedback to synchronize all oscillators and stabilize the frequency. The mutual coupling between the devices in the array is governed by the

---

[1] Naval Air Warfare Center, Weapons Division, China Lake, CA. 93555.

[2] On leave from University of Adelaide, Australia.

geometry of the grid. An advantage of this method of power combining is that the combining occurs in free space where the losses are close to zero. A theoretical analysis of the grid oscillator has been given by Popović et al. (2) and by Weikle (5), where an equivalent circuit for the grid in the quasi-optical resonator is presented, along with formulae for calculating equivalent circuit values.

This analysis has been used to design grids for operation between 25-40 GHz. Modifications to an ideal grid geometry were necessary to incorporate the high electron mobility transistor (HEMTs) millimeter wave sources at the lattice sites of the array. The nature of coupling as well as grid performance have been studied by fabricating grids with single device, 1x3, 3x1, 3x3 and 4x4 arrays. The grid design and the testing of the arrays are presented here.

Grid Design:

Following Weikle, the grid was modeled as an infinite two dimensional array with transistors set in a periodic fashion in two directions. Figure 1a shows the actual grid layout, which nearly fulfills our assumption. It is further assumed that each cell of the periodic grid with the transistor at the center is square and can be modeled as an equivalent waveguide with sides "a" and electric and magnetic walls at the boundaries as shown in Figure 1b. The vertical lines are drain and source connections and the horizontal line at the middle of the square is the gate control. The horizontal lines at the upper and lower boundaries are the drain and source bias lines. The inductance L due to vertical fingers used as drain and source millimeter circuit components, the distributed inductance L_m and the distributed capacitance C_m due to horizontal bias supply lines have been calculated. When these results are combined with the transistor parameters, the loop gain for the grid transistor oscillator can be obtained.

For a square unit cell of dimensions a, we obtain the inductance of the vertical finger leads from:

$$L(f,a) = \frac{a\mu}{\pi} \times \sum_{p=1}^{\infty} \frac{Sinc^2(p \cdot K)}{(\sqrt{(p^2 - f^2 a^2 \epsilon\mu)})} \qquad (1)$$

The distributed inductance due to the horizontal leads is:

$$L_m(f,a) = \frac{4\mu a}{(2\pi)^3} \sum_{p=1}^{\infty} \sum_{n=1}^{\infty} \frac{(Sin(nM)\,Sinc(pK)\,Sinc(nQ))^2}{[p^2+(n/2)^2]} \times \frac{[(2p/n)+(n/(2p(1-w/a)))]^2}{\sqrt{[(p^2+(n/2)^2-(fa)^2\epsilon\mu]}} \qquad (2)$$

and the distributed capacitance due to horizontal lines is:

$$\frac{1}{C_m(f,a)} = \frac{1}{a\pi\epsilon}\left[\sum_{n=1}^{\infty}\left(\frac{2}{n}Sin(nM)\,Sinc(nQ)\right)^2 \times \sqrt{\left[\left(\frac{n}{2}\right)^2-(fa)^2\epsilon\mu\right)} + 2\sum_{n=1}^{\infty}\sum_{p=1}^{\infty}(Sin(nM)\,Sinc(pK)\,Sinc(nQ))^2 \times \left(\frac{\sqrt{\left[p^2+\left(\frac{n}{2}\right)^2-(fa)^2\epsilon\mu\right)} \times (1-1/(1-w/a))^2}{p^2+(n/2)^2}\right)\right] \qquad (3)$$

where p=m/2 and m and n are TE and TM mode numbers, K=πw/a, M=π/2, Q=πw$_s$/2a, a is the unit cell size, w and w$_s$ are the widths of the vertical and horizontal lines and are set to 0.1a, f is the frequency, ϵ is the substrate dielectric constant and μ is the permeability of the substrate.

Figure 2 shows L as a function of frequency and unit cell size. The vertical lead inductance, L, is a relatively slowly varying function at low frequencies, but as the frequency approaches a particular value for each unit cell size, L rapidly increases to infinity. Above this frequency L is complex and below it L is real. We have plotted only the real part of L, since it is the real part of the inductance that directly couples with the fields. The imaginary part of the inductance appears to be associated with evanescent modes. The value of L slowly increases with increasing unit cell size as can be observed from equation 1. The discontinuities in this figure indicate where L becomes infinite; however, it appears as finite because of the incremental steps of calculation. The heights of the discontinuities in this figure are not very significant, but their positions indicate the frequencies at which the impedances associated with vertical fingers pass through resonance. Figure 3 shows a similar plot for L_m. Both the frequency and unit cell size dependencies are similar to figure 2.

The distributed capacitance C_m of the grid due to the horizontal lines was similarly calculated and is shown in figure 4. Here even though C_m has a similar behavior to L and L_m, the first singularity occurs at a much lower frequency, that is, for given parameters, C_m becomes complex at a much lower frequency than L and L_m.

In evaluating grid parameters, we found that the above calculation provides an acceptable means of obtaining L, L_m and C_m at frequencies well below the singularities, but not in their vicinities. Immediately below their singularities these parameters vary rapidly and one cannot extract an accurate value for them at a given frequency.

The singularities occur because a term in the denominator of each expression becomes zero at a particular frequency. In equation 3, the lowest frequency at which C_m increases rapidly and becomes complex, occurs when p=0 and n=1 and:

$$[(n/2)^2 - (fa)^2\mu\epsilon]^{1/2}=0$$

$$f=[2a(\mu\epsilon)^{1/2}]^{-1} \qquad (4)$$

which is the resonant frequency of a half wave dipole antenna. Based on this method, we have calculated the frequency and spectral dependance of grids and have designed, fabricated and tested them.

Grid Fabrication and Cavity Design:

Quartz was used as the substrate material based on the requirement of having a substrate material with a low dielectric constant, high heat conductivity as well as chemical compatibility with photolithography techniques. For this study, we have used substrates with thicknesses from 1.0 to 2.5 mm corresponding to dimensions equivalent to $\lambda/4$ to $5\lambda/8$ of the radiating fields.

RF sputtering was used to deposit chrome-gold metallization on quartz substrates, which were then electroplated to 2 μm with gold. This thickness is over four skin depths of gold at Ka-band. Photolithographic techniques were employed to pattern the metallization. The HEMT chips which have dimensions of 0.45 mm X 0.34 mm were then die attached to the gate bias line at the center of each unit cell. The electrical connections to the HEMTs are made by wire bonding the drain, source and gate to the grid using 0.7 mil gold wire. The width of the grid lines is one tenth of the unit cell size or 0.2 mm to 0.3 mm. This is considerably less than the size of the HEMT chip, which forced us to deviate from an ideal symmetric grid in order to keep the source connections parallel with the gate and drain connections. Figure 5 shows the bonding and placement of a single HEMT in the final grid design.

The drain, source and gate pads along the edges of the grid were wired to external power supplies. We have used ferrite beads on each connecting wire to eliminate low

frequency oscillations. This assembly was attached to a polished aluminium plate which was also the back reflector of the Fabry-Perot resonator. The front reflector is a spherical partially reflecting mesh whose details are given elsewhere (6). This reflector had a reflectivity of 85% and was placed about 25 cm away from the grid. The resonator was tuned by adjusting the position of the back reflector relative to the front reflector. Figure 6 presents a schematic diagram of the power combining cavity assembly.

The sources used are Mitsubishi MGFC-4414 pseudomorphic HEMTs with gate length of 0.3 μm and gate width of 150 μm. These devices are low-noise transistors with a unity gain frequency of greater than 60 GHz. Since our goal was to demonstrate feasibility of power combining at Ka-band, these transistors fit our requirements.

Figure 7 presents a schematic of the test and measurement system. After a grid was installed within the resonator and connected to the power supplies, the signals were collected by a lens and focused into a horn. A 10dB directional coupler provides input to a spectrum analyzer via a mixer and IF amplifier. The rest of the output was fed to a thermistor to measure power. We estimate that the measuring system intercepts 20% of the power radiated by the grid oscillator.

Results and Discussion:

Grid oscillators of various dimensions were fabricated and tested. As a test of Weikle's formulation, which assumes plane TEM waves incident on the grid, we performed reflectance measurements from 30 GHz to 50 GHz on designed grids and compared these results with the calculated values. Details of the technique have been published previously (7). The magnitude and phase of the reflectance for three different grid designs are shown in Figures 8a, 8b, and 8c along with a comparison with the model. Figures 8a and 8b show measurement results of earlier grid designs and figure 8c shows the results of the final grid design. A comparison of the data shows that as the grid designs deviated from an ideal symmetric grid, the magnitude and phase of the reflectance deviated from the theoretical model and as we refined the grid design by extending the vertical fingers a better agreement with the model was achieved. Based on these measurements we designed the final grid geometries.

To test Equation (4), grids of different unit cell size were evaluated. To coarsely measure the grid oscillation frequency, we placed a wavemeter in series with the power meter and searched for a dip in the magnitude of the signal by tuning the wavemeter from 26 to 40 GHz and in a separate

assembly from 18 to 26 GHz to look for the absence of subharmonics. Further we tuned the open resonator length and found that oscillations appeared at $\lambda/2$ intervals. Table 1 lists the results of these evaluations. Figure 9 shows a plot of the frequency dependence of Equation (4) compared with the experimentally determined oscillation frequencies of the grids fabricated in this work, as well as those in the literature.

Table 1. Grid arrays tested in Ka-band.

Grid array	Unit cell size (mm)	Predicted Frequency (GHz)	Measured frequency (GHz)
3x3	2.0	38	37.4
1x3	2.5	30	29.3
1x3	3.0	25	24.8
1x3	2.15	35	
1x3	2.3	33	

From the above results it is apparent that the dominant factor in frequency determination is the grid geometry and specifically the unit cell size. Other factors such as the active device, the Fabry-Perot cavity and the grid line widths have lesser influence. It should be stated that this frequency is for an unobstructed grid coupled to the free space within or outside the open resonator. Placement of the grid within a closed cavity that alters the effective impedance at the grid will change this frequency to a lower value.

Figure 10 shows the spectra of the 1x3 grid with 2.5 mm unit cell. Figure 10a indicates a narrow spectrum, while Figure 10b shows the purity of the signal. The spectra of Figure 10 is nearly the same for a single HEMT in the grid or for 1x3 or 3x3 arrays. This is another indication that the grid geometry is the dominant factor in frequency and spectrum determination.

The oscillation frequency was tunable over 12 MHz by either the gate bias or the cavity tuning, however this tuning was at the expense of a decrease in output power. Figure 11 shows the electronic tuning range for a 3x3 grid at 37.4 GHz.

In measuring the radiated power from the grid outside the cavity, it is estimated that less than 20% of the radiation is intercepted. Considering that the grid radiates into one half of free space, with an impedance of 377Ω, any

disturbance of this arrangement by placing a collector horn near the grid alters the impedance that is presented to the transistor grid and hence a reduction in output power may occur. We have measured the emitted power from the 1x3 array by bringing a high gain horn in close contact with the ground plane and measured 8 mW of output power. The grid was operated at 2.5 V drain to source bias and 53 mA, which results in 6% DC to RF conversion efficiency. It should be noted that this is the minimum power radiated by the grid. When the grid is oscillating in the open resonator or in unobstructed free space, the output RF power and efficiencies should be higher.

To study the role of substrate thickness on the power we varied the substrate thickness from 1.5 to 2.5 mm ($3\lambda/8$ to $5\lambda/8$) and observed the variation shown in Figure 12. The peak power appears at a substrate thickness of $\lambda/2$. The line through the data points is empirical.

Conclusions:

We have designed, fabricated and tested a series of planar grid oscillator arrays at Ka-band. The experimental frequency determinations agree well with those obtained for half wave dipole antenna resonances. The fabricated grids oscillate at 37.4, 29.3 and 24.8 GHz. We have obtained 8 mW of power from a 1x3 array with 6% DC to RF conversion efficiency.

We acknowledge the US Army Research Office and SDIO/US Army Strategic Defense Command support for funding this work under contract number DAAL03-91-G-0160. Opinions, interpretations, conclusions and recommendations are those of the authors and are not necessarily endorsed by the US Army.

References:

1. James W. Mink, "Quasi-Optical Power Combining of Solid State Millimeter Wave Sources" IEEE Trans. Microwave Theory Tech., MTT-34, pp. 225-279, February, 1986.

2. Z. B. Popović, R. M. Weikle, II, M. Kim, and D. B. Rutledge, "A 100 MESFET planar grid oscillator," IEEE Trans. on Microwave Theory and Techniques, Vol. 39, Feb. 1991, pp. 193-200.

3. Z. B. Popović, R. M. Weikle, II, M. Kim, K. A. Potter, and D. B. Rutledge, "Bar Grid Oscillators," IEEE Trans. on Microwave Theory and Techniques, Vol. 38, Mar. 1990, pp. 225-230.

4. R. M. Weikle, II, M. Kim, J. B. Hacker, M. P. DeLisio, and D. B. Rutledge, "Planar MESFET Grid Oscillators Using Gate Feedback," IEEE Trans. on Microwave Theory and Techniques, Vol. 40, Nov. 1992, pp. 1997-2003.

5. R. M. Weikle, II, "Quasi-optical Planar Grids for Microwave and Millimeter-Wave Power Combining," Ph.D. thesis, California Institute of Technology, 1992.

6. H. M. Harris, A. Torabi, R. W. McMillan, C. J. Summers, J. C. Wiltse, S. M. Halpern, and D. W. Griffin, "Quasi-Optical Power Combining of Solid State Sources in Ka-Band," accepted for presentation at the IEEE MTT-S International Microwave Symposium, Atlanta, Georgia, June 15, 1993.

7. D. R. Gagnon, "Highly Sensitive Measurements with a Lens Focussed Reflectometer," IEEE MTT-S International Symposium Digest, Vol. 3, pp. 1017-108, Boston, Ma., 1991.

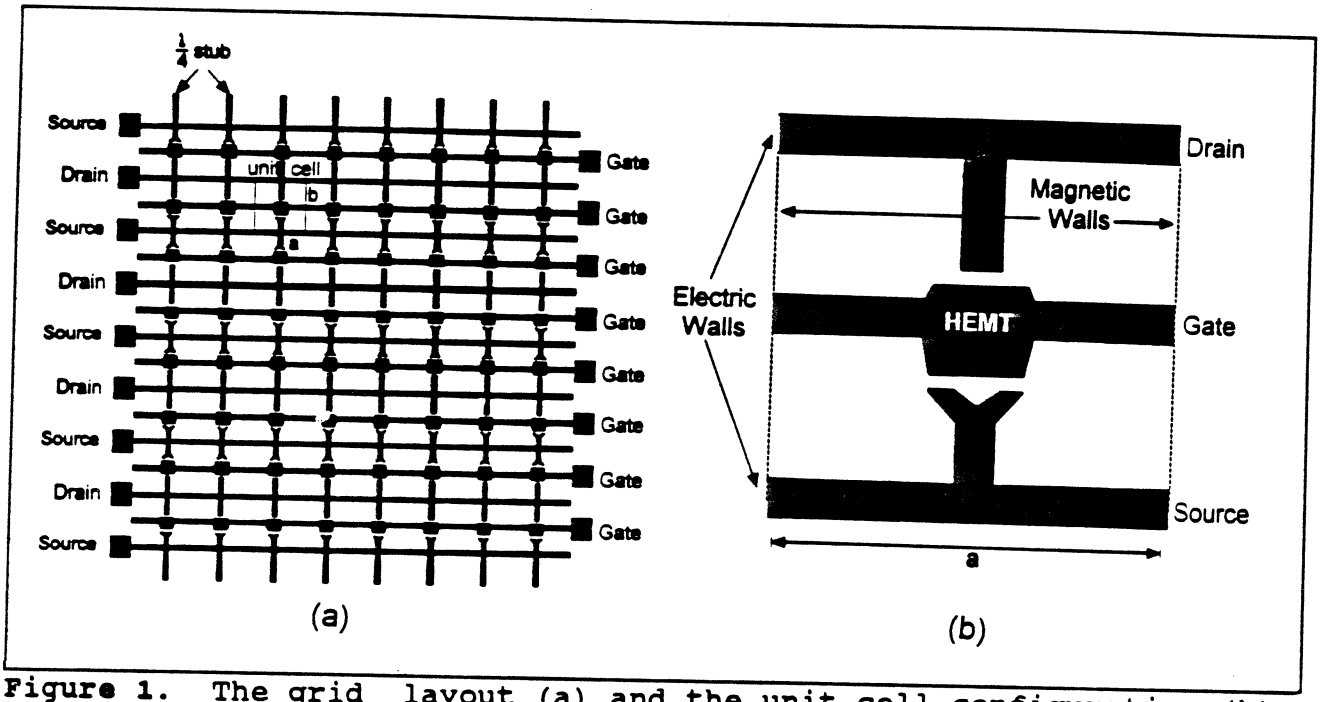

Figure 1. The grid layout (a) and the unit cell configuration (b).

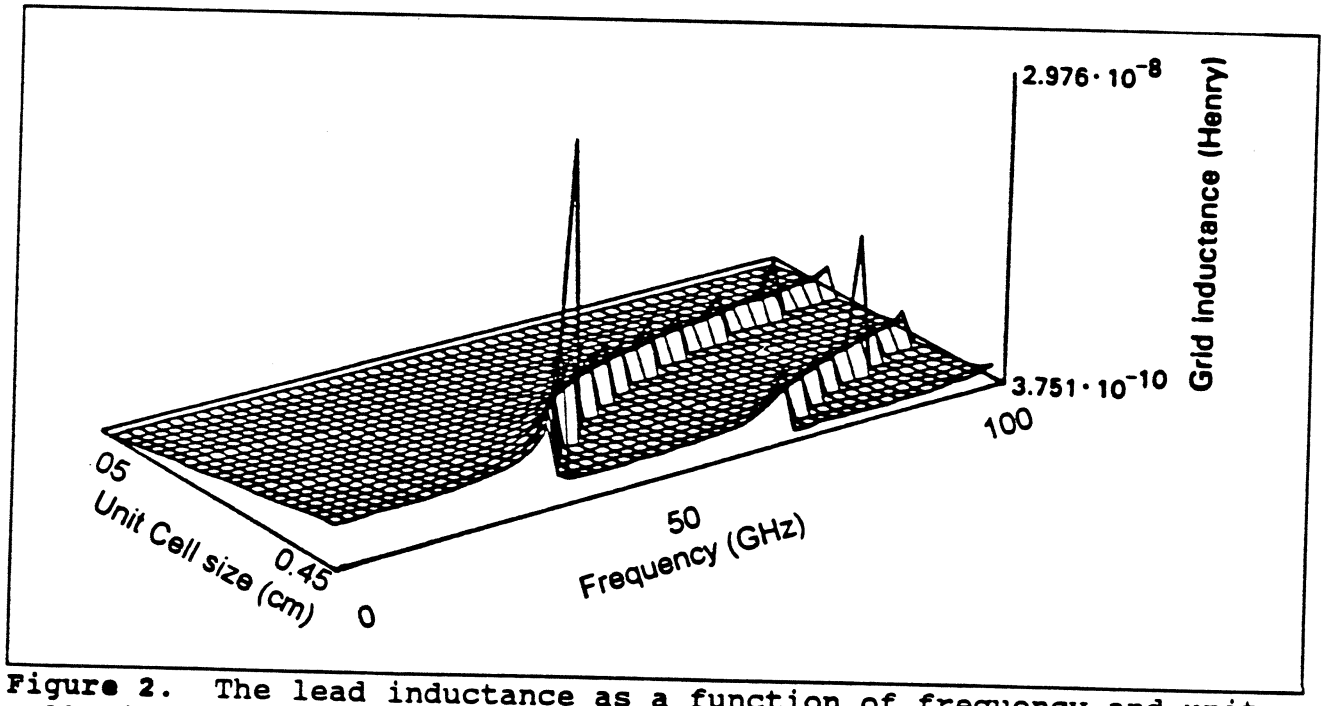

Figure 2. The lead inductance as a function of frequency and unit cell size.

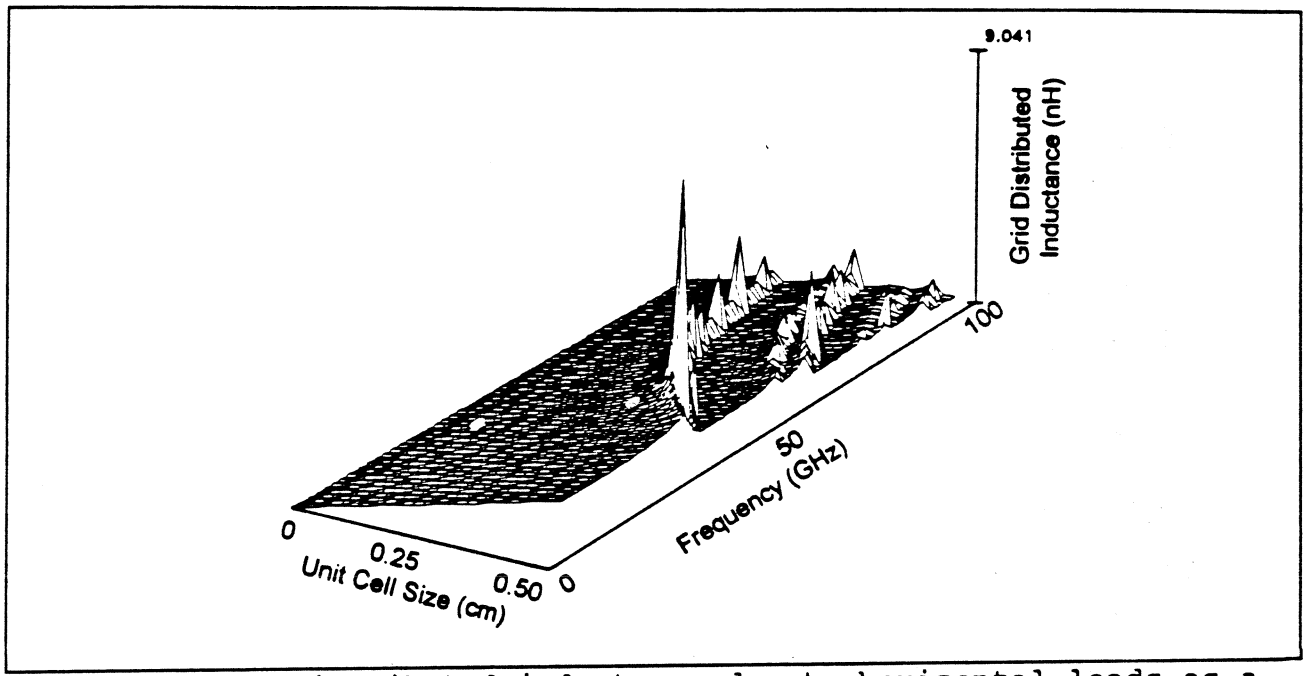

Figure 3. The distributed inductance due to horizontal leads as a function of frequency and unit cell size.

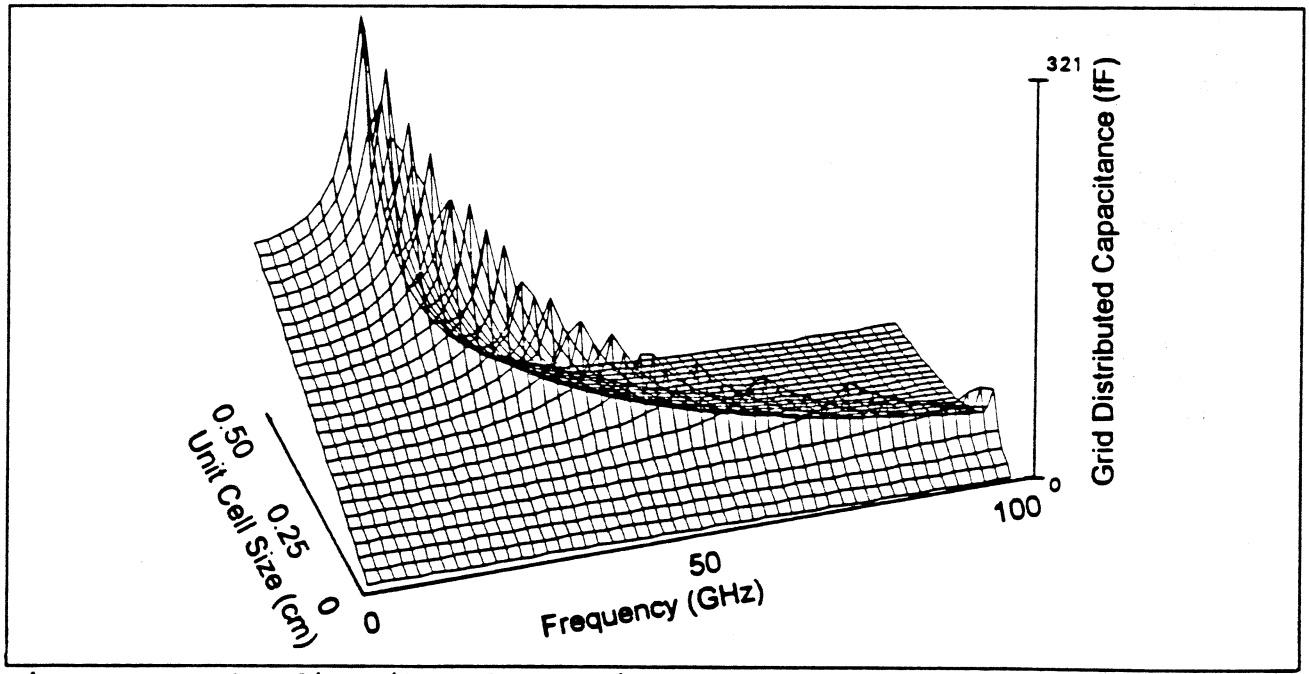

Figure 4. The distributed capacitance due to horizontal leads as a function of frequency and unit cell size.

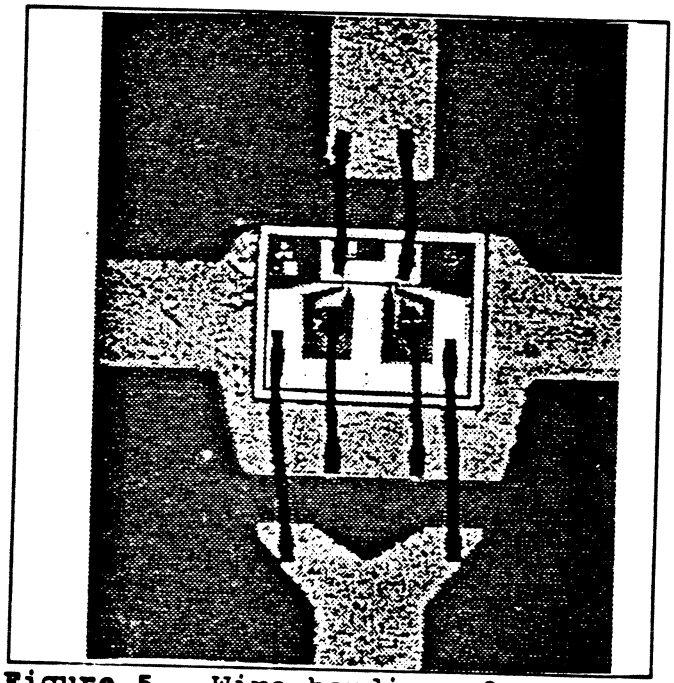

Figure 5. Wire bonding of a HEMT in the grid oscillator array.

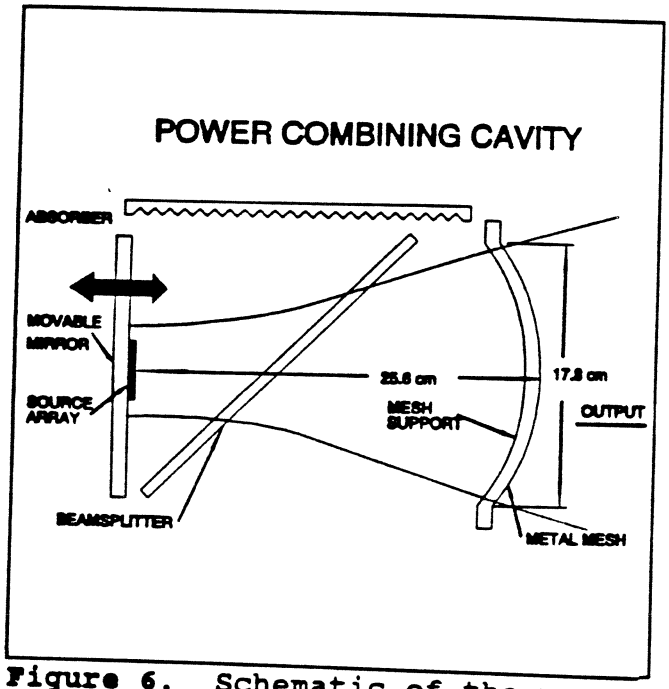

Figure 6. Schematic of the power combining cavity.

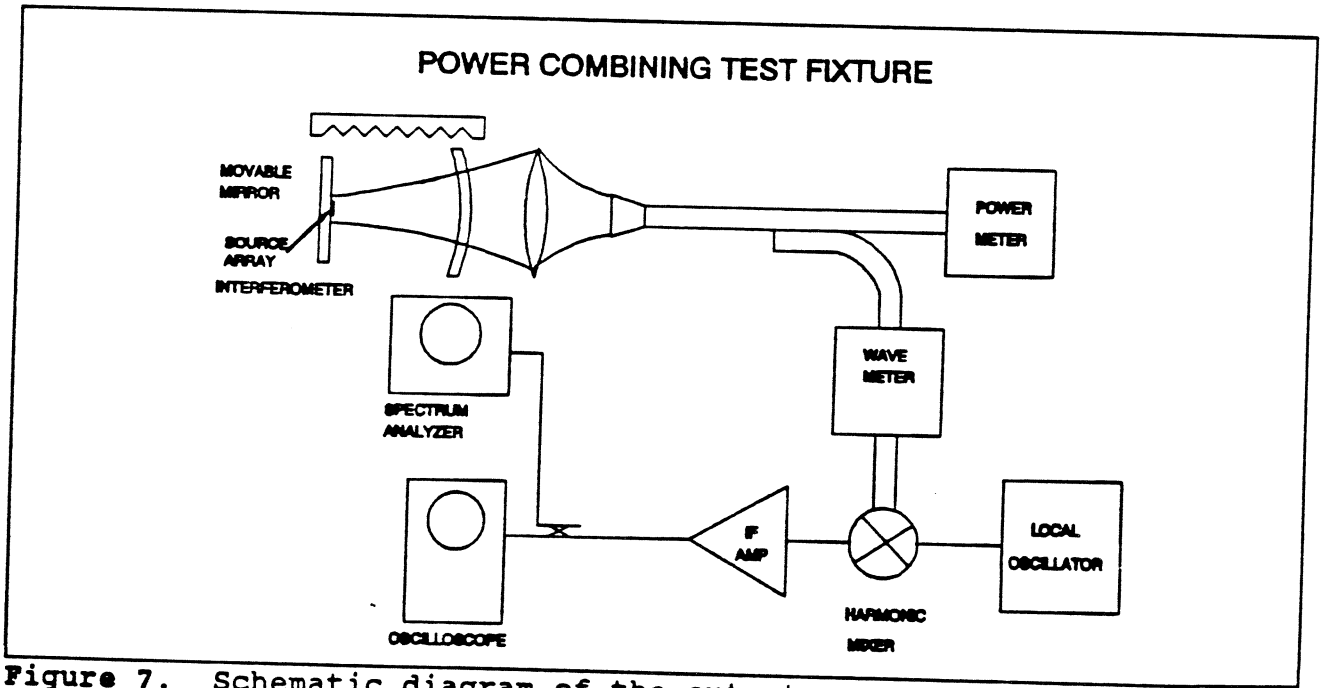

Figure 7. Schematic diagram of the output power and spectrum measurement system.

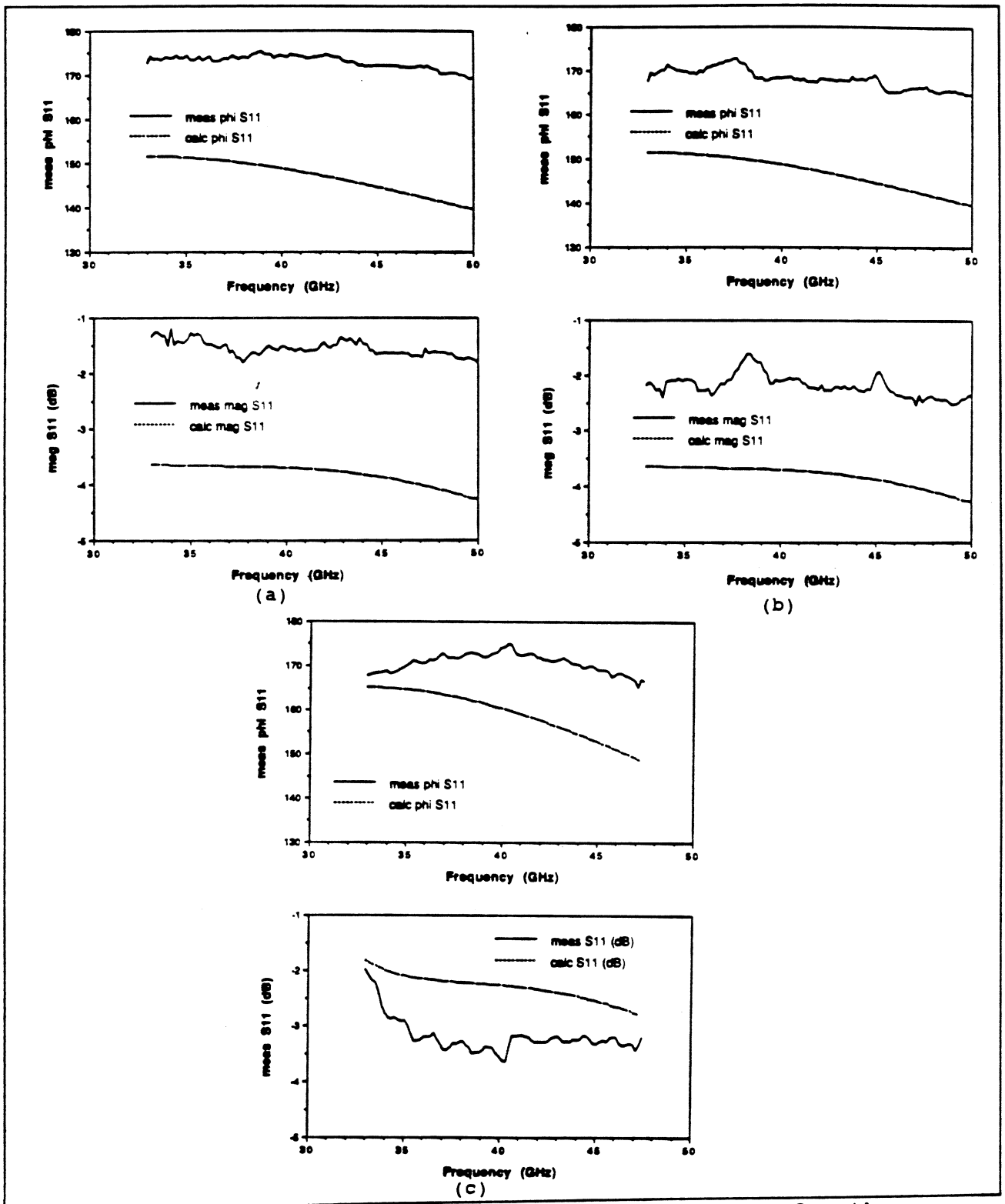

Figure 8. The magnitude and phase of the reflectance for three different grid designs. Design (c) was used in the final grid.

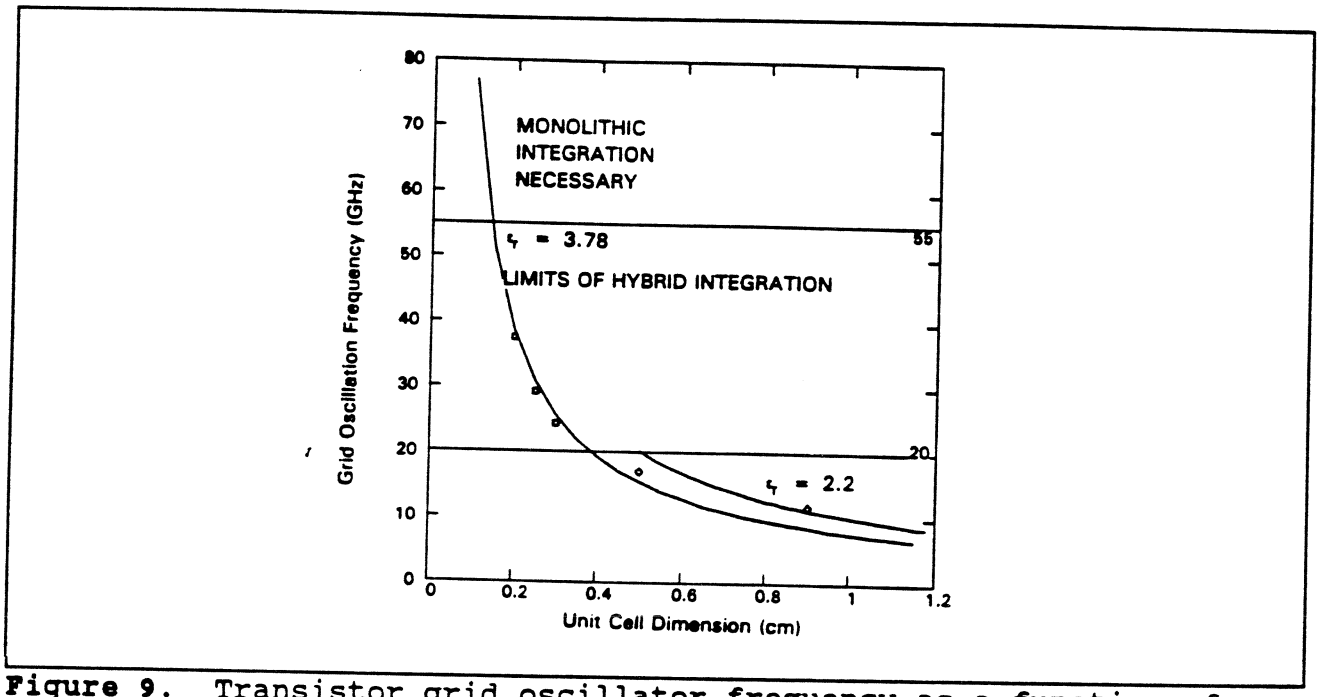

Figure 9. Transistor grid oscillator frequency as a function of unit cell size. The squares are experimentally measured frequencies and the diamonds are from reference 5.

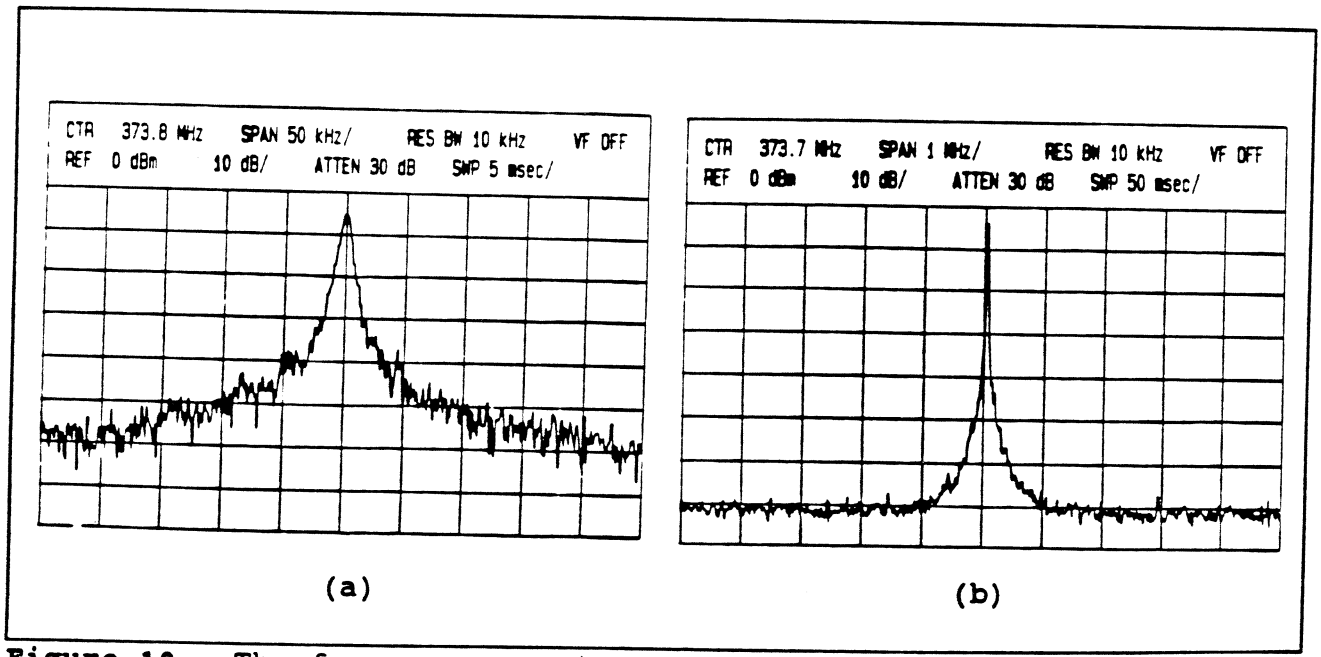

Figure 10. The frequency spectra measured for a 1x3 grid oscillator.

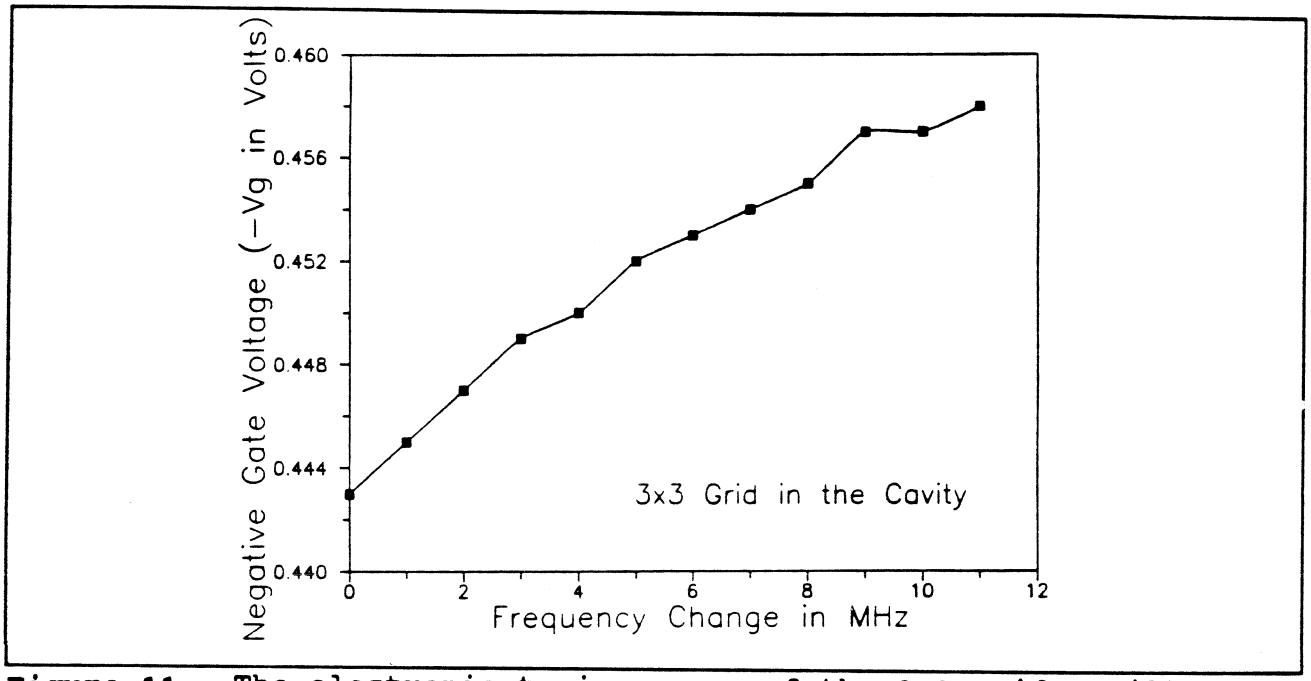

Figure 11. The electronic tuning range of the 3x3 grid oscillator.

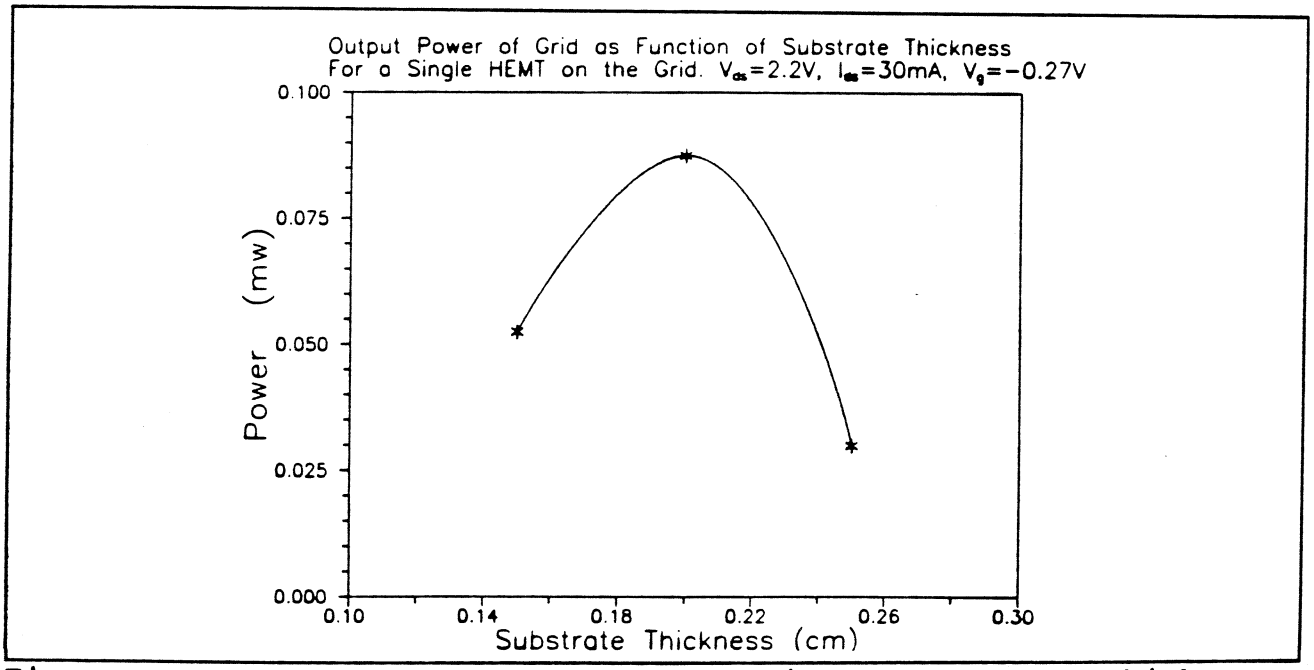

Figure 12. The measured power as a function of substrate thickness.